Experimental and computational evaluation of the thermohydraulic performance of compact, gravity-driven, closed-loop thermosyphon cooling systems

Guilherme Armas
Department of Chemical Engineering
Instituto Superior Técnico
Lisbon, Portugal
guilherme.armas@tecnico.ulisboa.pt

***Abstract*— A passive loop thermosyphon cooling system was tested at different heat loads, filling ratios and volumetric air flow rates for two low global warming potential working fluids: R1233zd(E) and R1234ze(E). The prototype, with a height of 66 mm and a 61 x 56 mm^2 microchannel evaporator, was tested on a 40 x 40 mm^2 (16 cm^2) copper block heated surface. Several filling ratios were tested. The optimum charge of refrigerant was found to be in 40-60% range. The thermosyphon was tested for R1233zd(E) and a filling ratio of 46% at heat loads from 100 W to 700 W and volumetric air flow rates from 40 CFM to 178 CFM, yielding junction temperatures between 34°C and 92°C. Another set of tests, comparing the performance of R1234ze(E), at 51% filling ratio, with R1233zd(E), at 41% filling ratio, for heat loads from 50 W to 500 W, and volumetric air flow rates from 40 CFM to 118 CFM yielded similar junction temperature for both fluids, between 32°C and 92°C. Thermal resistance values as low as 0.081°C/W were reached.**

For several tests, a drop in performance in the left side of the device was observed, and this was confirmed by an X-ray microtomography scan to be related to partial internal blockages on that side of the device.

The cold start-up and transient behaviour of the device was also analysed, showing the overall stability of the system, except for some minor disturbances at high filling ratios and low heat loads.

Keywords— loop thermosyphon, cooling system, heat recovery, two-phase flow

NOMENCLATURE

CPU – central processing unit, -

LTS – air cooled loop thermosyphon cooling system, -

GDR – gravity dominant regime, -

FDR – friction dominant regime, -

FR – filling ratio, %

MPT – multiport tube, -

TIM – thermal interface material, -

VI – virtual instrument, -

$A_{copper\ block}$ – copper block cross-section area (16 cm^2)

k_{Cu} – copper thermal conductivity (398 Wm^{-1}K^{-1})

L_{block} – distance between the TTop thermocouple (top level, centred thermocouple in the copper block) and the junction (2 mm)

q_{cond} – copper block heat transfer rate, W

U – voltage, V

I – current, A

p_{atm} – atmospheric pressure (101325 Pa)

$A_{anem.}$ – anemometer cross-section area (78.5 cm^2)

v_air – air velocity, measured by the anemometer, m/s

$\Delta P_{mom.}$ – momentum pressure drop, Pa

$\Delta P_{friction}$ – frictional pressure drop, Pa

ρ – density, kg/m^3

Q_{in} – inlet air volumetric flow rate, CFM

TR – thermal resistance, °C/W

h – thermosyphon height, m

g – gravitational acceleration, m/s^2

$T_{air,in}$ – average inlet air temperature, °C

I. Introduction and Literature Review

The use of two-phase cooling technologies, because of the high heat transfer coefficient associated with boiling/condensing flow, has been increasingly researched for high heat flux applications, such as the cooling of servers in data centres [1], fuel cells [2] or electronics on commercial aircraft [3]. These applications require the removal of large amounts of heat in a limited space, for which two-phase cooling can be taken advantage of. In the case of data centres/servers, the conventional approach is direct air-cooling using fans. Due to the low heat transfer coefficient for air cooling, this approach implies high air flow rates and pressure drops, and consequently high-power consumption due to the fans. In addition, the sustainable development goals for the next decades provide an incentive for waste heat recovery, which can be done through integration of these technologies with existing power plants and district heating networks [4]. In this scope, the development of passive two-phase cooling technologies by introducing a gravity-driven thermosiphon loop can help mitigate these problems, by increasing the fluid-side heat transfer coefficient and hence reducing the overall footprint of the system.

This work discusses the thermohydraulic behaviour of a loop thermosyphon that relies on the boiling of a fluid in a microchannel evaporator in contact with a heat source, which then rises to a condenser section where it condenses by rejecting the latent heat into a heat sink.

Significant work on this topic has been performed over the last two decades. Bieliński *et al.* (2011) [5] have concluded that there are two dependences of the mass flow rate on the heat flux in a loop thermosyphon: at lower heat loads, the gravity dominant regime (GDR), where the mass flow rate increases with increasing heat load; and the friction dominant regime (FDR), where the increase in heat flux decreases the mass flow rate. In addition, very low filling ratios can cause partial or intermittent dry-out of the evaporator (lower CHF), and very high filling ratios can cause flooding of the thermosyphon, both of which decrease heat transfer performance [6].

Tests with R134a at filling ratios between 38-87% and heat fluxes between 35-400 W/cm^2 in a loop thermosyphon with a total length of 2.04 m were performed by Liu *et al.* (2018) [7]. A section of the loop was used as the evaporator. They concluded that the lowest thermal resistances (below 0.2°C/W) were observed for filling ratios between 40-60% and higher heat loads. A peak in thermal resistance was observed around 70% FR: the lower values for lower filling ratios are caused by the enhanced heat transfer resulting from the increased relevance of latent heat transfer; the decreasing values at higher filling ratios are explained by the formation of a two-phase flow continuum between the riser and evaporator. The thermal resistance also decreased with increasing heat load: due to both the mass flow and latent heat transfer increase. They also did a detailed study on the types of instabilities and performance issues for different conditions: low filling ratios, despite increased thermal performance, might exhibit transient instabilities due to localised near dry-outs in the evaporator; intermediate filling ratios, at heat fluxes high enough to generate bubbles of comparable size to the riser, but not high enough to generate a driving force to compensate the riser liquid column, cause an intermittent bubble coalescence and liquid propelling known as geyser boiling; high filling ratios, due to the low

compressibility of the liquid phase, allow an increase in pressure at higher heat loads, leading to a high subcooling and dangerously high pressures.

Garrity *et al.* (2009) [2] studied a loop thermosyphon, for use in fuel cell cooling, with heights between 0.79 and 1.33 m, using a microchannel evaporator, heat fluxes up to 7 W/cm^2 and HFE-7100 as the working fluid. They proposed an explanation for instabilities, by defining two regions: one, for low pressure drops and vapour quality in the evaporator, where pressure drop increases with increasing flow rate and the gravitational driving force decreases with increasing flow rate (higher mass flow implies a lower vapour quality), leading to a negative feedback loop and stabilising the system; and another region, at higher evaporator pressure drops and vapour qualities, where increasing the flow rate decreases the pressure drop, causing a positive feedback either until the mass flow rate is high enough and the vapour quality low enough, and the system goes into the stable zone again, or until circulation ceases. This difference in behaviour is mostly explained by the fact that pressure drop increases with increasing vapour quality until it reaches 60-90%, and then decreases for higher values [8]. These last authors, on the other hand, have experimentally validated a simulator for a microchannel evaporator-thermosyphon system, with a height of 15 cm, for application to on-chip cooling of servers. The water-cooled system was tested at heat fluxes of 15-33 W/cm^2, a filling ratio of 67% and using R134a as the working fluid. They concluded, from simulation results, that there is a multiplicity of stationary states (mass flow rates) for the operation of the thermosyphon; this is typical of systems for which simultaneous complex energy and mass balances need to be solved, like polytropic reactors. And like in that case, only one of the stationary states is usually stable: for the ones at higher vapour qualities/lower mass flow rates, disturbances cause them to progress to a stable stationary state, as explained by Garrity *et al.* (2009) [2].

Amalfi *et al.* (2020) [9] characterised the thermal performance of a water-cooled loop thermosyphon with a total height of 70 mm and a 60 x 60 mm^2 microchannel evaporator. The device was tested on a 40 x 40 mm^2 pseudo-chip surface, for heat loads up to 200 W and using R1234ze(E) as working fluid. A maximum pseudo-chip temperature of 46°C was observed for 200 W of heat load (water coolant inlet temperature was set at 15°C). The thermal resistance generally decreased with increasing heat load, due to the enhanced boiling heat transfer from the increase in mass flux, vapour quality and heat flux. A minimum thermal resistance value of 0.113°C/W was reached for a heat load of 120 W. Further, simulation studies were performed and found that in the range of tested heat loads, the mass flow rate and vapour quality increased with increasing heat load, indicating that the thermosyphon was in the gravity dominant regime.

II. TEST RIG AND LOOP THERMOSYPHON DESCRIPTION

The tested device is a thermosyphon, built in aluminium, with approximate external dimensions of 213 x 56 x 65 mm and an internal volume of 90 cm^3. The thermosyphon was previously designed and fabricated (patent pending) by JJ Cooling Innovation for the cooling of a CPU in a data centre server. The overall microchannel evaporator cooling zone is approximately 50 x 50 mm^2, while the total base is approximately 61 x 56 mm^2. Above, 6 flat condenser tubes with internal microchannels are located, separated by louvered fins for cooling air flow and above that a cover plate (Fig. 1). This figure also

shows the scheme of the test rig, with the thermocouple positions and fluid patterns. The temperatures were measured using type K thermocouples: the copper block had 1 mm thermocouples inserted into its centre and fixed with thermal grease, the fin temperatures were measured by 0.5 mm thermocouples, and the remaining LTS temperatures were measured using thermocouples in adhesive tape. A Keller PA-33X absolute pressure transducer was connected to the top of the right riser. The thermocouples were calibrated against a Testo T480 reference probe in a LAUDA Proline AP885 thermal bath. The pressure transducer was calibrated using a YANTRIKA pneumatic dead weight tester.

The device was filled with a known charge of the working fluid, through the top left riser filling orifice. The cooling zone base of the LTS was pressed against the copper block serving as a heat source, and the cool air flowed through the louvered fins to remove the heat. The air is drafted through a set of SanAce 9CRA0612P6K001 fans and its mean velocity was measured by a Testo T480 anemometer. On top of the LTS, a pressure system applied a known imposed vertical pressure to the LTS to firmly set the thermal interface material (TIM) between the copper heating block and the evaporator. After fixing the evaporator on top of the copper block with 6 cartridge heaters inserted into its base, the fluid is partially vapourised in the evaporator, creating a two-phase flow into the risers, where it flows upwards and into the multiport tubes (MPTs) of the condenser, which are connected to a set of fins, through which the air flows to remove the latent heat generated in the evaporator. After cooling, the fluid flows into the downcomer, from where it returns, completely liquid, into the evaporator.

The thermocouple and transducer signals were acquired through a NI SCXI380 terminal module using a LabVIEW virtual instrument in a personal computer. This VI also automatically set, in a predetermined order, the power in the cartridge heaters and the inlet air flow (based on anemometer measurements).

Using the acquired data, the temperatures in the two sides of the LTS, in addition to the junction temperature and thermal resistance. The junction temperature, *i.e.,* the temperature in the interface of the copper block with the TIM can be estimated by:

$$T_{Junction} = TTop - q_{cond}\frac{L_{Block}}{k_{Cu}A_{copper\ block}} \quad (1)$$

The dissipated heat is determined from the voltage and current applied by the power supply:

$$q_{cond} = UI \quad (2)$$

Additionally, the thermal resistance between the junction and the inlet air temperature was also calculated:

$$TR_{LTS+TIM} = \frac{T_{Junction} - T_{air,\ in}}{q_{cond}} \quad (3)$$

The inlet air volumetric flow rate was determined from the air velocity measured by the anemometer and corrected for the density at the inlet of the air-side LTS:

$$Q_{in} = v_{air}\,A_{anem.}\frac{\rho_{out}(TAirOut,\ p_{atm})}{\rho_{in}(T_{air,in},\ p_{atm})} \quad (4)$$

III. Uncertainty analysis

Using the partial derivatives method for uncertainty propagation, the uncertainty associated with the heat load, junction temperature and thermal resistance were determined (*viz.* equations 5 to 7).

$$\varepsilon_{q_{cond}}^2 = U^2\varepsilon_I^2 + I^2\varepsilon_U^2 \quad (5)$$

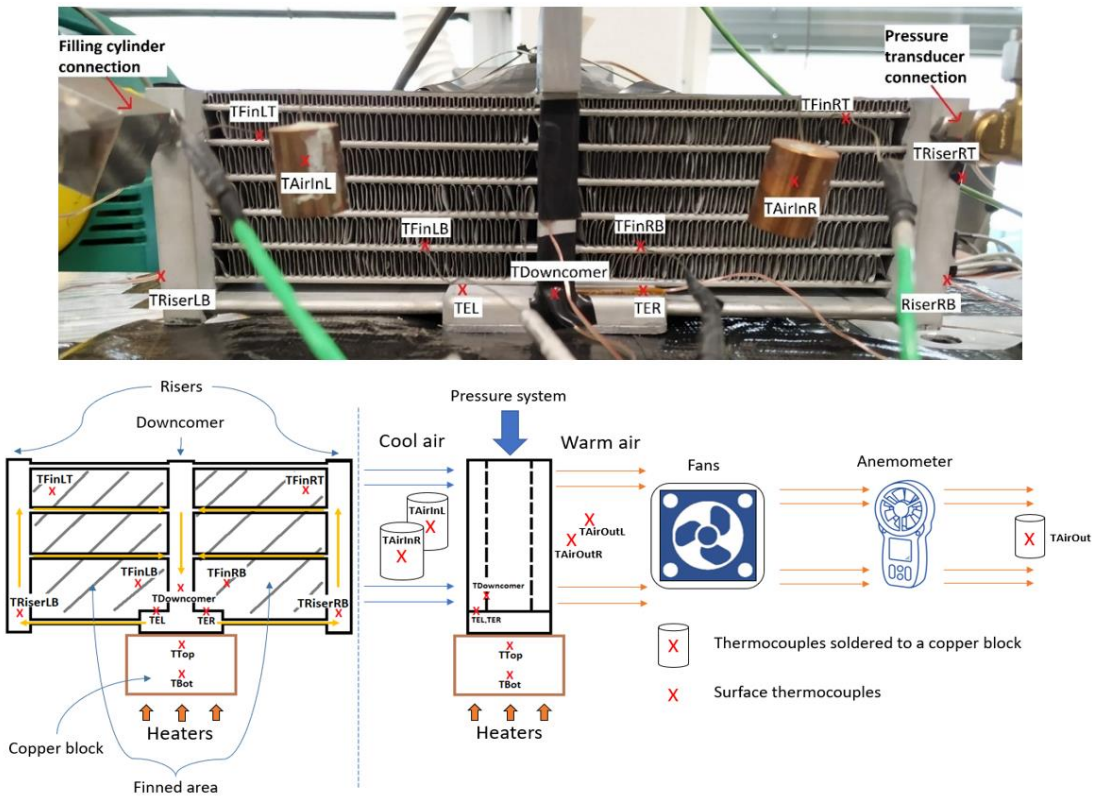

Fig. 1. Designed and prototyped LTS showing thermocouples and pressure transducers locations (top). Scheme of the experimental facility, showing thermocouples locations and the main and secondary fluids flow directions (bottom)

$$\varepsilon^2_{T_{Junction}} = \varepsilon^2_{TTop} + \left(\frac{L_{Block}}{k_{Cu}A_{copper\ block}}\right)^2 \varepsilon^2_{q_{cond}} \quad (6)$$

$$\varepsilon^2_{TR} = \left(\frac{\sqrt{2}\varepsilon_T}{q_{cond}}\right)^2 + \frac{(T_{Junction} - T_{Air,in})^2}{q^4_{cond}} \varepsilon^2_{q_{cond}} \quad (7)$$

The temperature uncertainty is a combination of the maximum difference between the thermocouples and the reference probe at 25°C after calibration (±0.25°C), the temperature probe uncertainty (±0.1°C) [11], and the fluctuations at each steady state (±0.35°C):

$$\varepsilon_T = \pm\sqrt{0.25^2 + 0.1^2 + 0.35^2} = \pm 0.44℃ \quad (8)$$

Analogously, the uncertainty associated with a temperature difference is:

$$\varepsilon_{\Delta T} = \sqrt{2}\varepsilon_T = \pm 0.62℃ \quad (9)$$

IV. Experimental Results

A. Optimal filling ratio

The optimum working fluid filling ratio was determined, for R1233zd(E) and R1234ze(E), under conditions of constant heat load and several air volumetric flow rates. The inlet air temperature was between 24-27°C for R1233zd(E) and 25-29°C for R1234ze(E).

The lowest junction temperatures and thermal resistance values (*viz.* Figs. 2 and 3) were achieved for filling ratios between 40-60% for both fluids. R1233zd(E) could not be tested below 30% FR and R1234ze(E) not below 40% FR because the junction temperature would have exceeded 100°C.

An equivalent analysis was done for a constant air volumetric flow rate of 95 CFM and three different heat loads for R1233zd(E). The corresponding thermal resistance values are shown in Fig. 4.

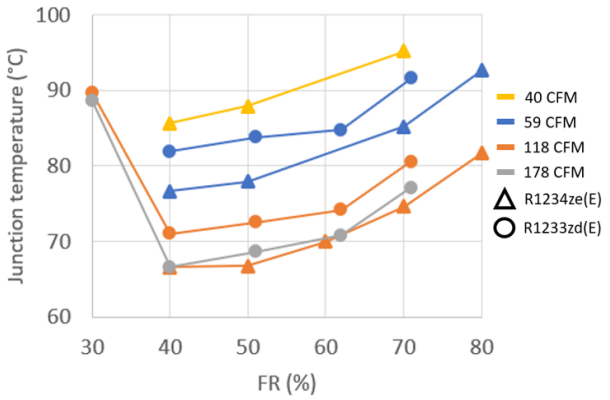

Fig. 2. Junction temperature for different filling ratios and inlet air volumetric flow rates, for 500 W of heat load and both working fluids

The junction temperature was able to be kept at 85°C for the lowest air volumetric flow rate at a 40% filling ratio and 500W of heat load. Secondly, the thermal resistances achieved go well below 0.1°C/W and as low as 0.081°C/W for the highest air volumetric flow rate.

Fig. 5 shows the left and right riser temperatures for both working fluids. A particular trend observed is that, for 60-70% FR range, the left riser temperature drops abruptly (especially for R1233zd(E)) to values close to ambient temperature for the higher air flow rates.

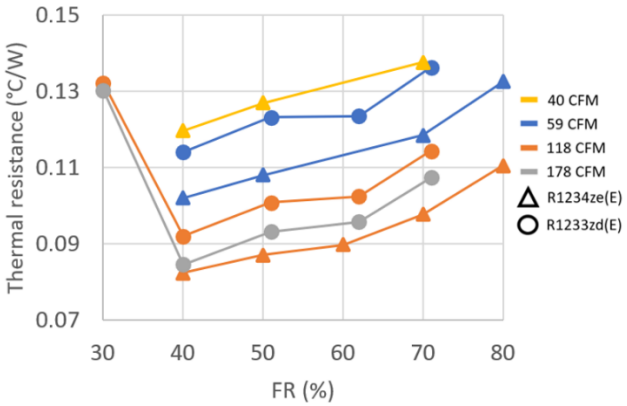

Fig. 3. Thermal resistance for different filling ratios and air flow rates, at a heat load of 500 W (31.25 W/cm^2) and both working fluids

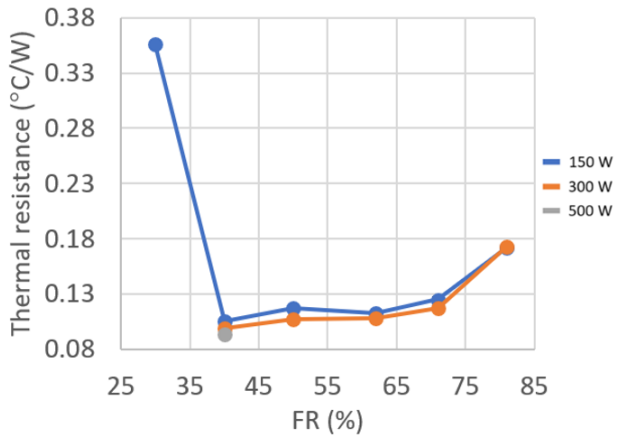

Fig. 4. Thermal resistance for different filling ratios and heat loads, at an inlet air flow rate of 95 CFM and both working fluids

This potentially indicates that the working fluid flow might have slowed or stopped in the left side of the LTS, as a result of a higher left side flow resistance. A microtomography scan (3D metal X-ray) was done, and this confirmed that some partially and some completely blocked channels were observed in the left-side MPTs, especially in the upper ones. This both reduces the driving force (left-side term on Eq. 10) of the thermosyphon and increases the frictional pressure drop, when compared to the right side [6]:

$$(\rho_{downcomer} - \rho_{riser})gh = \Delta P_{friction} + \Delta P_{mom.} \quad (10)$$

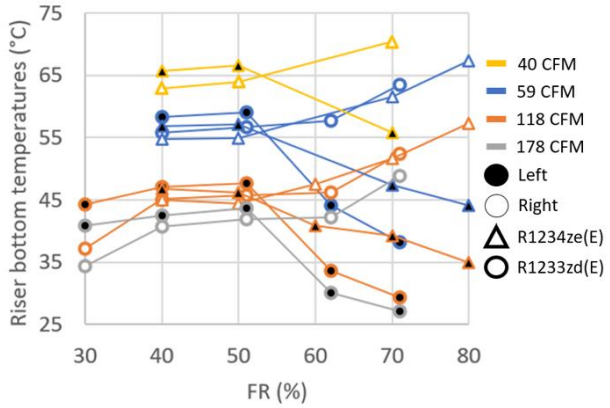

Fig. 5. Riser temperatures (TRiserLB and TRiserRB) for different filling ratios and air volumetric flow rates, at a heat load of 500 W (31.25 W/cm^2) and both working fluids

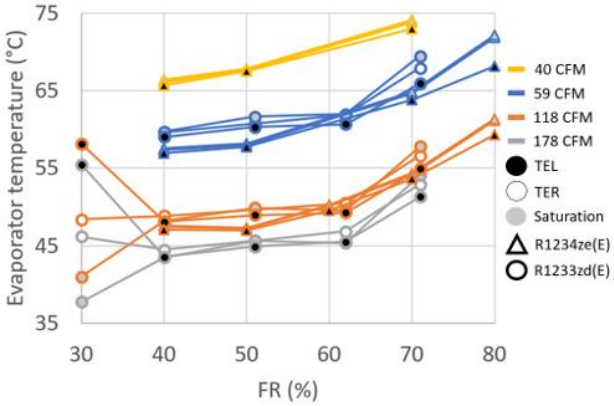

Fig. 6. Evaporator and saturation temperatures (TEL and TER) for different filling ratios and air flow rates, at a heat load of 500 W (31.25 W/cm^2), for both working fluids

Finally, Fig. 6 shows the temperatures on the evaporator cover plate (left and right sides), as well as the saturation temperature. The temperatures are close to the saturation temperature.

An exception is the low filling ratio of 30% and R1233zd(E), where both sides are considerably above saturation, especially the left side, potentially indicating superheating. However, since the left riser is below saturation (Fig. 5), this likely means that there is a localised dry-out of the evaporator, more relevant in the left side, with the increased temperature in the evaporator cover plate due to conduction from the copper block through the metal, and not to superheating. Partial dry-outs are common for lower filling ratios [6][7]. Furthermore, there is significant subcooling at 80% FR, for both working fluids; this is also common for high filling ratios, because the higher volume of liquid allows for higher pressures to be reached [7].

B. *Thermal performance experimental campaign for the optimum filling ratio*

The optimum charge was determined to be between 40 and 60% FR for both fluids, and R1233zd(E) and R1234ze(E) reach too high temperatures below 30% and 40% FR, respectively. Therefore, tests were performed at charges of 41% FR for R1233zd(E) and 51% FR for R1234ze(E), with inlet air temperatures of 25-27°C and 27-29°C, respectively, and 3 levels of air volumetric flow rate. The observed values for junction temperature and thermal resistance are shown in Figs. 7 and 8. The junction temperatures are similar for both fluids; however, the thermal resistances are slightly lower for R1234ze(E), especially for higher air flow rates.

The minimum observed thermal resistance, 0.081°C/W, was observed for R1234ze(E) when applying 500W of heat load and 118CFM of air volumetric flow rate. For all cases, it seems that the thermal resistance decreases with increasing heat load. However, especially for lower air volumetric flow rates, a plateau seems to be reached, which can be an indication of the transition from GDR to FDR.

Fig. 9 shows the difference in the increase in temperature between the right and left sides of the LTS:

$$\Delta\Delta T = (TAirOutR - TAirInR) - (TAirOutL - TAirInL) \quad (11)$$

The air temperature seems to increase more on the right side of the LTS, and this difference is most pronounced for R1234ze(E) at low air flow rates.

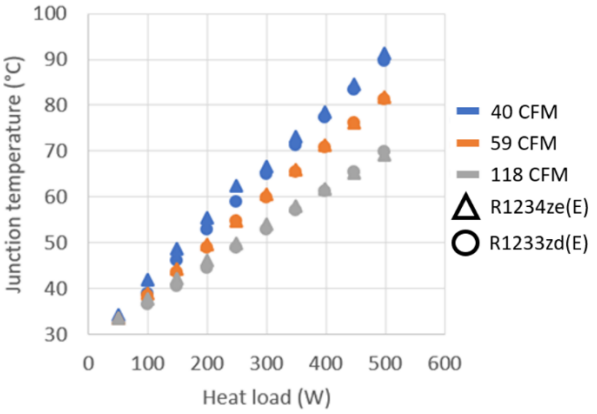

Fig. 7. Junction temperature values for three air flow rates and heat loads between 50-500 W (both working fluids)

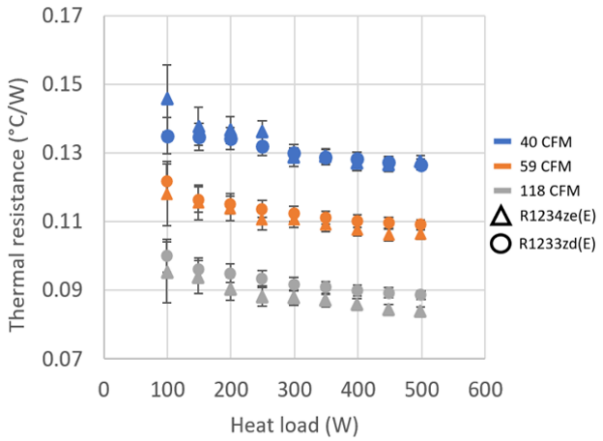

Fig. 8. Thermal resistance values for three air flow rates and heat loads between 50-500 W, for both working fluids

On the other hand, the thermal resistance had already been shown to be slightly lower for R1234ze(E). It is unclear how this can be explained: if on the one hand R1234ze(E) has a viscosity 3 times lower than R1233zd(E), which should reduce frictional pressure drop, it also has a lower density in the liquid phase, which decreases the driving force for circulation. These effects would have to be studied in more detail, and a specific model would need to developed to take into account the internal asymmetry of the LTS.

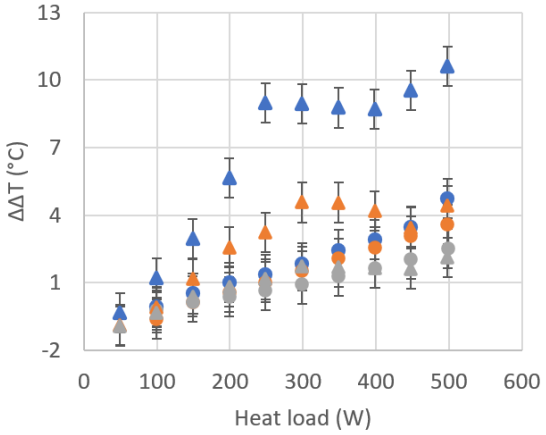

Fig. 9. Right minus left side difference of the increase in temperature, for three air flow rates and heat loads between 50-500 W, for both working fluids.

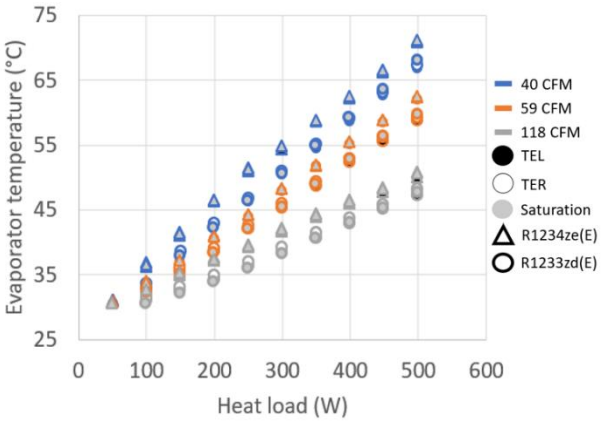

Fig. 10. Evaporator and saturation temperatures for 3 values air volumetric flow rates and heat loads between 50-500 W, for both working fluids

Fig. 10 shows that the evaporator cover plate temperatures are similar for both fluids and close to the saturation temperature.

Finally, an additional set of tests was performed for the working fluid R1233zd(E) at 46% FR, air volumetric flow rates between 89-178 CFM, and inlet air temperatures between 26-29°C. As can be seen in Fig. 11, a heat load of 700 W was reached while maintaining the junction temperature below 87°C.

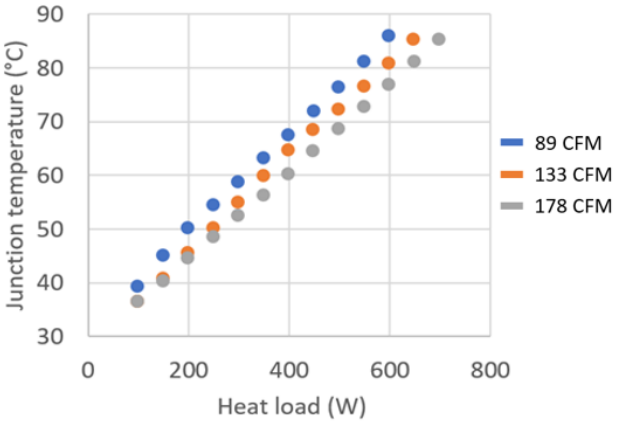

Fig. 11. Junction temperature values for R1233zd(E) at 46% FR and heat load up to 700 W

C. *Transient behaviour*

In addition to the previous results, obtained for each stationary state, an analysis of the transient behaviour is also provided. Fig. 12 shows the measured temperatures of the LTS along the time and considering the start-up from 0 to 150 W and then to 300 W at a time of 4100 s. The results presented are for R1233zd(E) as working fluid, 80% FR, and 95 CFM for air volumetric flow rate. It can be seen that the temperatures rise smoothly for the first step in power. The same can be said for the second step in power, but with a slight overshoot and a small oscillation with a period of around 40 s.

These oscillations may simply correspond to the LTS oscillating between two possible states, one of which is inherently unstable [8] [2].

The start-up behaviour for other filling ratios and conditions is similar to the start-up to 150 W, without any overshoots, although with slightly more or less fluctuations depending on the case.

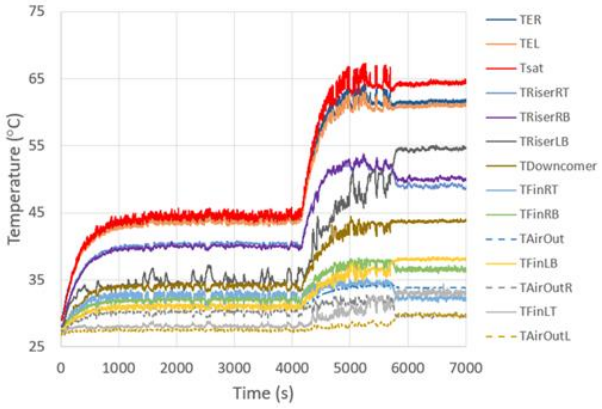

Fig. 12. Start-up behaviour for R1233zd(E) at 80% FR and 95 CFM of inlet air flow, first from 0 to 150 W, and then from 150 to 300 W

V. Conclusions

The test results for the loop thermosyphon device with two refrigerant fluids, R1233zd(E) and R1234ze(E), showed an optimum filling ratio range of 40-60%, for a wide range of heat loads and air flow rates. It also showed a significant asymmetry between the right and left sides of the LTS: for filling ratios around 60-70%, circulation seems to cease in the lefts side, as indicated by the abrupt decrease in the left riser temperature. This suggested internal blockages in the left side, which were confirmed by an X-ray microtomography scan.

Testing at the optimum charges (41% FR for R1233zd(E) and 51% FR for R1234ze(E)) showed, for both working fluids, a decrease in thermal resistance with increasing heat load, with a plateau for values higher than 300W, in the case of the lowest air volumetric flow rates. This is probably explained by the increase in internal mass flow, vapour quality and heat flux, increasing the boiling and condensation heat transfer coefficients. The plateau at heat loads above 300 W might indicate the beginning of the transition from GDR to FDR. In addition, the air appears to heat more on the right side, reinforcing the better performance on this side. R1234ze(E) seems to show a slightly lower thermal resistance for most air flow rates, but also shows a higher asymmetry in air heating between the two sides, for lower air flow rates.

Finally, the system seems to be fairly stable, with slightly more oscillations at lower power levels, and a more relevant oscillation for an increase in heat load at 80% FR with R1233zd(E), where cyclic oscillations, probably due to the system oscillating between two possible stationary states.

References

[1] J. Cao, Z. Zheng, M. Asim, M. Hu, Q. Wang, Y. Su, G. Pei and M. Leung, "A review on independent and integrated/coupled two-phase loop thermosyphons," Applied Energy, vol. 280, 2020.

[2] P. T. Garrity, J. F. Klausner and R. Mei, "Instability phenomena in a two-phase microchannel

thermosyphon," International Journal of Heat and Mass Transfer, vol. 52, pp. 1701-1708, 2009.

[3] C. Sarno, C. Tantolin, R. Hodot, Y. Maydanik and S. Vershinin, "Loop thermosyphon thermal management of the avionics of an in-flight entertainment system," Applied Thermal Engineering, vol. 51, pp. 764-769, 2013.

[4] J. B. Marcinichen, J. A. Olivier and J. R. Thome, "On-chip two-phase cooling of datacenters: Cooling system and energy recovery evaluation," Applied Thermal Engineering, vol. 41, pp. 36-51, 2012.

[5] J. Bieliński and H. Mikielewicz, "Natural Circulation in Single and Two Phase Thermosyphon Loop with Conventional Tubes and Minichannels," in Heat Transfer - Mathematical Modelling, Numerical Methods and Information Technology, vol. 19, InTech, 2011, pp. 475-496.

[6] N. Lamaison, C. L. Ong, J. B. Marcinichen and J. R. Thome, "Two-Phase Thermosyphon Cooling of Datacenters," in Encyclopedia of Two-Phase Heat Transfer and Flow III - Macro and Micro Flow Boiling and Numerical Modeling Fundamentals, Vols. 3 - Micro-Two-Phase Cooling Systems, World Scientific, 2018.

[7] Y. Liu, Z. Li, Y. Li, Y. Jiang and D. Tang, "Heat transfer and instability characteristics of a loop thermosyphon withwide range of filling ratios," Applied Thermal Engineering, vol. 151, pp. 262-271, 2018.

[8] N. Lamaison, C. L. Ong, J. B. Marcinichen and J. R. Thome, "Two-phase mini-thermosyphon electronics cooling: Dynamic modeling, experimental validation and application to 2U servers," Applied Thermal Engineering, vol. 110, pp. 481-494, 2017.

[9] R. L. Amalfi, F. Cataldo and J. R. Thome, "The Future of Data Center Cooling: Passive Two-Phase Cooling," Electronics Cooling, pp. 16-21, Summer 2020.

[10] Keysight Technologies, "Keysight N5700 Series Data Sheet" 2017.

[11] Testo, "Digital temperature, humidity and air flow meter" 2020. [Online]. Available: https://www.testo.com/en-TH/testo-480/p/0563-4800.